3.2 APT AND TEM CHARACTERIZATION OF PRECIPITATES IN Mg^+ ION IMPLANTED CUBIC SILICON CARBIDE

— W. Jiang, J. Liu, D. K. Schreiber, D. J. Edwards, C. H. Henager, Jr., R. J. Kurtz (Pacific Northwest National Laboratory), and Y. Wang (Los Alamos National Laboratory)

OBJECTIVE

This study aims to characterize precipitates and defect structures in Mg^+ ion implanted and high-temperature annealed cubic silicon carbide (3C-SiC).

SUMMARY

This research update reports on the results from our preliminary atom probe tomography (APT) data reconstruction and analysis as well as from our recent transmission electron microscopy (TEM) examinations on Mg^+ ion implanted cubic silicon carbide (3C-SiC). APT studies have been performed for 3C-SiC implanted with $^{25}Mg^+$ ions to 9.6×10^{16} ions/cm^2 at 673 K and subsequently annealed at 1073 and 1573 K for 2, 6, and 12 h. TEM examinations have been focused on a lower-dose (5.0×10^{15} ions/cm^2) 3C-SiC implanted with $^{24}Mg^+$ ions, followed by annealing at 1573 K for 12 h. The TEM study suggests that some of the nanometer-scale Mg precipitates are associated with Frank loops in the implanted and annealed 3C-SiC, while the APT results show that most of Mg-bearing particles contain both Si and C. Further efforts on APT reconstruction and TEM examination are still in progress.

PROGRESS AND STATUS

Introduction

Elemental transmutation of silicon in silicon carbide due to high-energy neutron irradiation leads to production of magnesium, a major non-gaseous transmutant as predicted by Sawan, *et al*. [1]. The presence of the transmutants and irradiation-induced defects in 3C-SiC are expected to affect its thermomechanical properties, which needs to be investigated prior to application of the material in fusion reactors. As an on-going study, we continue to investigate the formation and behavior of Mg-bearing precipitates in 3C-SiC using ion implantation and thermal annealing methods. Our previous study [2] suggests that precipitates of cubic Mg_2Si and tetragonal MgC_2 are likely formed in 3C-SiC implanted to 9.6×10^{16} $^{25}Mg^+$/cm^2 at 673 K and subsequently annealed at 1573 K for 12 h. These precipitates were not observed directly, but derived from fast Fourier transformation (FFT) of an atomic-level resolution high-angle annular dark field (HAADF) scanning TEM (STEM) micrograph [2]. The APT method is currently being used to examine the possible precipitates. To facilitate APT analysis for differentiating Mg from $^{12}C_2$ clusters using time-of-flight mass spectrometry, isotope $^{25}Mg^+$ ion implantation has been performed. In addition, low ion fluence was also implanted for STEM studies of both initial Mg states in the nucleation process and possible formation of low-concentration voids that could be individually resolved.

Experimental Procedure

3C-SiC samples were implanted 7° off the surface normal with 200 keV $^{25}Mg^+$ ions at 673 K to a high ion fluence of 9.6×10^{16} ions/cm^2. This fluence corresponds to ~6 at.% ^{25}Mg and 54 dpa at their respective peak maxima (depths of 280 and 220 nm) based on SRIM simulations [3]. The isotope ^{25}Mg was obtained from the National Isotope Development Center (NIDC) at Oak Ridge and the implantation was performed at Los Alamos National Laboratory (LANL). An additional $^{24}Mg^+$ ion implantation was also performed at LANL to a lower fluence of 5×10^{15} ions/cm^2 at the same ion energy and sample temperature. The implanted samples were cleaved into smaller pieces for thermal annealing under different conditions. Each set of the low and higher dose samples was annealed at 1573 K for 2, 6 and 12 h in flowing Ar gas, respectively. Additional annealing of the $^{25}Mg^+$ ion implanted sample was also performed at 1073 K for 12 h for comparison of APT data. To minimize surface oxidation, the samples were placed inside a chimney made of a Ta metallic foil to reduce the oxygen partial pressure.

Both TEM and APT samples were prepared using a focused ion beam (FIB) microscope at the Pacific Northwest National Laboratory. Once finished, the APT samples were quickly put into the ultrahigh vacuum chamber of the APT to avoid contamination. APT examinations were carried out at a sample temperature of 44 K and a bias voltage ranging from 5.5 to 8.5 kV with a laser power of 60 – 80 pJ/pulse at a frequency of 125 kHz. The detection efficiency was 36% with an average detection rate of 0.4%, i.e., 4 detected evaporation events in 1000 pulses. Three to four APT needles were prepared from each of the unimplanted, as-implanted, and implanted and annealed samples. The total ions collected for each needle range from 3 to 5 M ions. Some of the needles fractured during APT measurements. The measured C and Si concentrations are not calibrated. For unimplanted high-purity 3C-SiC single crystals, Si to C ratio is shown as being about 60:40 and this ratio can change slightly for different measurements due to selective loss of C at the detector. TEM was performed using a Cs-corrected JEOL ARM 200 CF TEM/STEM microscope. Equipped with a cold field emitter, the microscope is capable of sub-Å spatial resolution under HAADF STEM imaging. The high-brightness source coupled with a ~0.3 eV energy resolution allows for a fast acquisition of electron energy loss spectroscopy (EELS) and energy dispersive x-ray spectroscopy (EDS) analyses. EELS and EDS utilize the latest Gatan Quantum 965 spectrometer with Dual EELS and a proprietary JEOL Centurio Si-drift EDS detector with 0.98 Sr collection angle from a detection area of 100 mm^2, respectively. EDS measurements in selected areas and elemental mapping with automatic sample drift corrections were performed at both 200 kV and 80 kV, the latter of which was used to minimize sample damage.

Results

Figure1(a) shows a bright-field TEM image from the peak damage region in 3C-SiC implanted to 5.0×10^{15} $^{24}Mg^{+}/cm^{2}$ and subsequently annealed at 1573 K for 12 h. A high-concentration of small Frank loops is

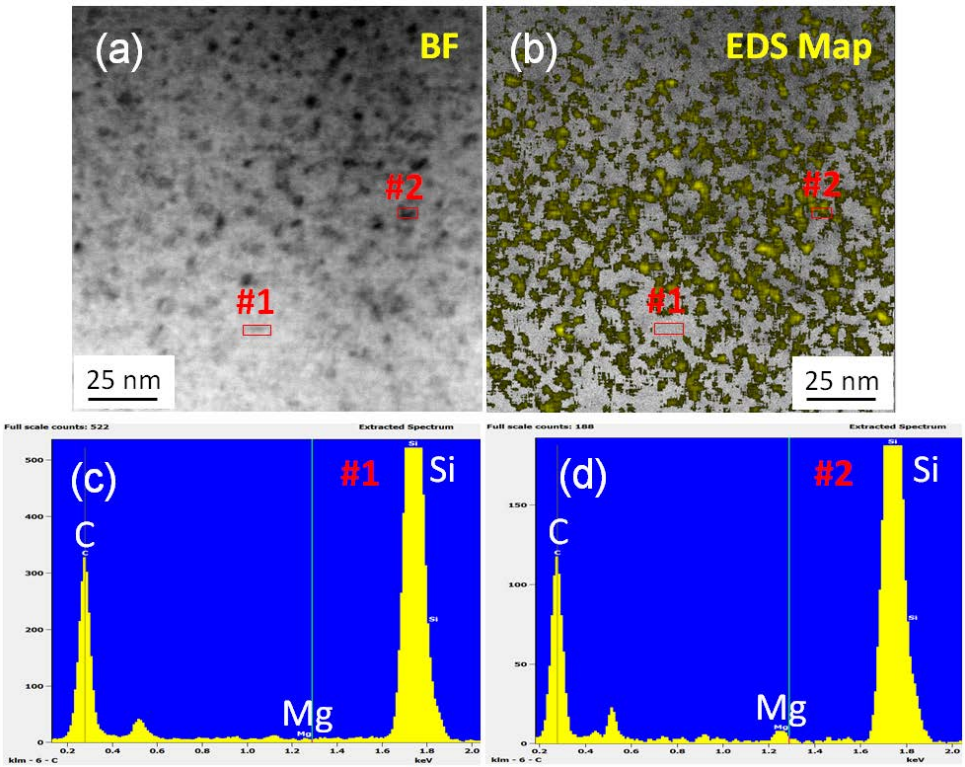

Figure 1. (a) Bright-field TEM image, (b) EDS map for implanted Mg, and (c) and (d) EDS spectra from Mg-deficient and Mg-rich areas, respectively, in the Mg profile peak region of 3C-SiC implanted to 5.0×10^{15} $^{24}Mg^{+}/cm^{2}$ and annealed at 1573 K for 12 h.

observed. Over the same area, EDS mapping for Mg was performed and the result is shown in Figure 1(b). Although the concentration of the implanted Mg at the peak is small (~0.1 at./cm^3 Mg), Mg clustering to a size on the order of a few nanometers is evident in the sample. The brighter area represents a higher local Mg concentration. Figures 1(c) and 1(d) show EDS spectra at spots #1 and #2 from Mg-rich and Mg-deficient regions, respectively. A close inspection reveals that some of the Mg clusters exhibit a location correspondence with the Frank loops. An example is shown at spot #2 in Figures 1(a) and 1(b). A more detailed study of the location relationship between Mg clusters and dislocation loops is currently being pursued using the APT method. Further atomic-level resolution TEM examinations are planned to study the initial states of Mg nucleation in 3C-SiC and the possible formation of voids in 1573 K annealed samples.

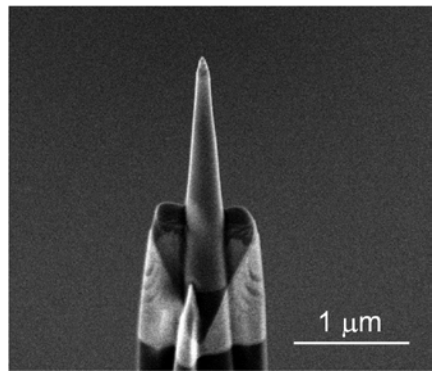

Figure 2. SEM image of the final APT needle, prepared using FIB from 3C-SiC implanted to 9.6×10^{16} $^{25}Mg^{+}/cm^{2}$ and annealed at 1573 K for 12 h.

The APT measurements have been performed for various 3C-SiC samples, including as-received (unimplanted), as-implanted (9.6×10^{16} $^{25}Mg^{+}/cm^{2}$ at 673 K), and post-implantation annealed at 1073 K for 12 h and at 1573 K for 2, 6 and 12 h. A systematic APT data reconstruction analysis is currently being conducted for those measurements and the results are intended for a journal publication. Here, we report the preliminary results for the annealed sample at 1573 K for 12 h only. Figure 2 shows the final shape of the sample prepared using a FIB. The apex of the needle is located at a depth of ~200 nm and the APT analytical range is ~200 nm in depth starting from the apex, which covers both the damage peak and Mg profile peak regions.

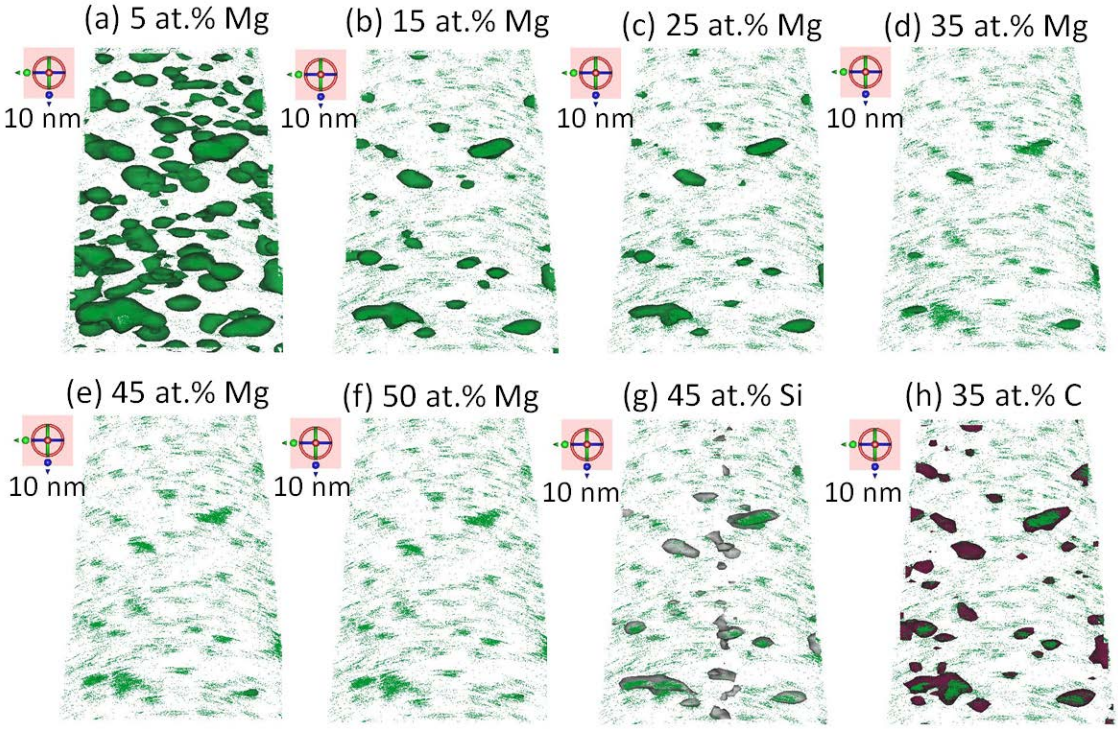

Figures 3. (a) – 3(f) show a sequence of iso-concentration surfaces of Mg at concentrations of 5 – 50 at.% Mg. The two-dimensional plots are obtained from a 10 nm slice of material in the Mg peak region. With increasing Mg iso-concentration threshold, Mg clusters become smaller, shrinking towards the cluster cores.

At 15 at. % Mg, the clusters are well resolved with a size up to 10 nm or larger. The Mg clusters completely disappear at the iso-concentration value of ~53 at.% Mg in this particular region of implantation. Figure 3(g) shows iso-concentration surfaces of Si at 45 at.% Si, overlapped with 100% of the detected Mg atoms also shown as green dots. The volumes encompassed by the surfaces represent the regions where there is a local Si depletion. As the Si concentration increases, the volume shrinks and diminishes to zero at 38 at.% Si (data not shown). The results suggest formation of a compound containing Mg and Si. From Figure 3(g), there are also regions where Si depletion [or enrichment (data not shown)] is not accompanied by noticeable Mg concentrations. These regions are probably formed due to irradiation-induced structural defects in 3C-SiC. Similarly, some of the C depleted regions shown in Figure 3(h) are also superimposed with Mg clusters, while other locations are not. By comparing Figures 3(g) and 3(h), it is evident that Mg-bearing particles are formed with Si, C or both. Further analysis of Mg to Si and Mg to C concentration ratios (data not shown) suggests that a great majority of the Mg-bearing particles contain both Si and C. Further APT analysis is being performed to visualize three-dimensional dislocation loops, which will be overlapped with Mg cluster maps, similar to a previous report on H^+ ion irradiated stainless steel [4].

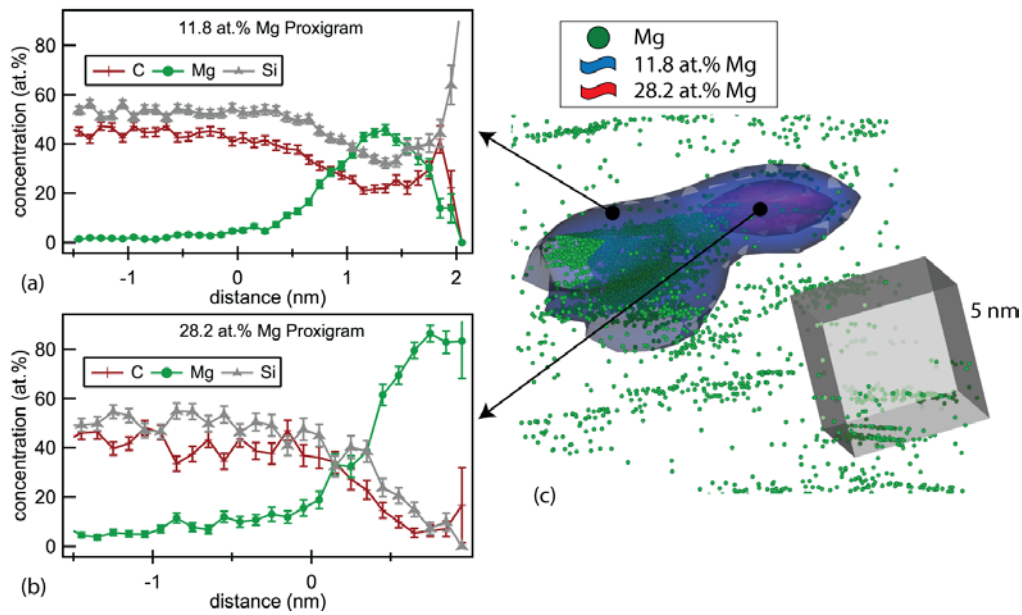

Figure 4. Proximity histograms from (a) 11.8 at.% Mg and (b) 28.2 at.% Mg iso-concentration surfaces of the same particle. (c) Corresponding atom map and iso-concentration surfaces. Error bars represent the standard deviation from counting error.

A representative analysis of a single relatively large Mg cluster is presented in Figure 4. Two different iso-concentration values (11.8 at.% Mg and 28.2 at.% Mg) were used to define the particle and generate proximity histograms. For the lower concentration, the apparent enrichment peaks at ~50 at.% Mg, whereas the higher concentration threshold reveals enrichment in excess of 80 at.% Mg. This suggests that this particle is approaching pure Mg, which is consistent with a previous TEM/EDS observation that appears to indicate that Mg aggregates within the volume of possible voids in 3C-SiC. Further TEM/EDS efforts are needed to verify this result. It should be noted that this particle does not exhibit a strong deviation from the nominal Si to C ratio, which implies that the particle is not approaching either a silicide- or carbide-like composition.

Estimation of Guinier's radii of Mg clusters has been attempted, which represent the feature size of precipitates in many metal compositions [4-6]. Figure 5 shows the result, indicating that the radius peaks at 0.3 – 0.4 nm with very few clusters larger than 2 nm. This radius distribution is not fully consistent with the TEM observation shown in Figure 1 and may not be representative of the physical cluster size distribution in the Mg^+ implanted SiC. Conventional cluster analysis [7] of the APT data was unable to determine a clear plateau to establish a d_{max} parameter in the cluster count distribution even using a very large order number (~50). This observation, in concert with the inconsistency with the TEM data, suggests that the conventional cluster size distribution analysis by APT has limitations and does not apply well in this study, probably as a result of the large field evaporation difference between Mg (~21 V/nm) and SiC (>33 V/nm).

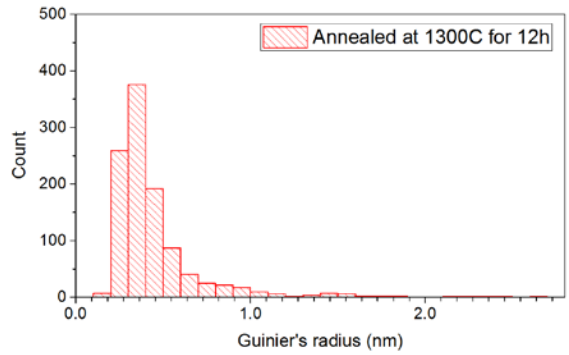

Figure 5. Guinier's radii of Mg clusters in 3C-SiC implanted to 9.6×10^{16} $^{25}Mg^+/cm^2$ and annealed at 1573 K for 12 h.

An alternative approach for analysis of the cluster distribution has been performed based on the change in the peak height (maximum cluster counts) in the nearest neighbor distribution as order number increases. The optimal order number is chosen at the minimum decrease in the peak height, from which d_{max} is determined. Figure 6(a) shows the cluster fraction profile as a function of the numbers of Mg atoms. The data are binned at a step of 100 atoms. The result shows that clusters containing 200 – 300 Mg atoms are most probable. Some of the clusters can contain 2000 Mg atoms or more. Similarly, for all atoms, including Si, C and Mg, the profile in Figure 6(b) shows similar features with 400 – 500 atoms at the peak. It should be noted that the analysis is parameter-optimized for larger clusters. Smaller clusters may be neglected and not be well reflected in the distributions shown in Figures 6(a) and 6(b). Figure 6(c) shows the composition distribution of the identified clusters. The most abundant clusters in the sample based on the analysis have a composition of ~50% Si, ~37.5% C and ~12.5% Mg.

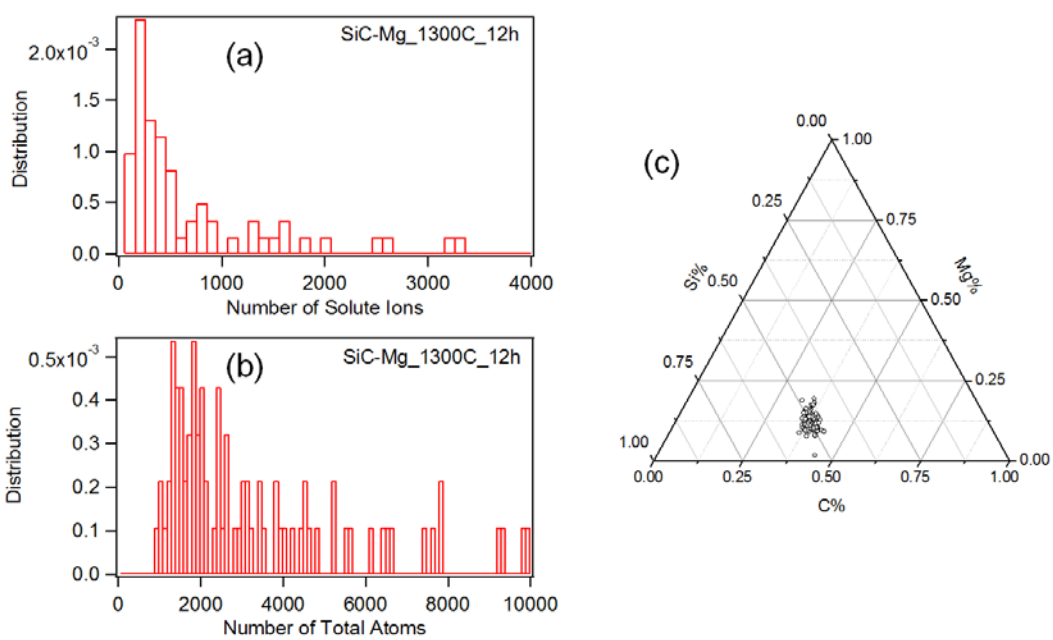

Figure 6. Distribution of the numbers of (a) Mg and (b) Si, C and Mg atoms in the identified clusters and (c) distribution of the cluster composition in 3C-SiC implanted to 9.6×10^{16} $^{25}Mg^+/cm^2$ and annealed at 1573 K for 12 h.

Acknowledgements

This research was supported by Office of Fusion Energy Sciences, U.S. Department of Energy (DOE) under Contract DE-AC05-76RL01830. Ion implantation was performed at the Ion Beam Materials Laboratory through partial support from the Center for Integrated Nanotechnologies (CINT), a DOE nanoscience user facility jointly operated by Los Alamos and Sandia National Laboratories. TEM and APT were performed under a general user proposal at the Environmental Molecular Sciences Laboratory (EMSL), a national scientific user facility located at PNNL. Isotope ^{25}Mg used in this research was supplied by the DOE Office of Science Isotope Program in the Office of Nuclear Physics.

References

[1] M. E. Sawan, Y. Katoh, and L. L. Snead, J. Nucl. Mater. 442 (2013) S370.
[2] W. Jiang, H. J. Jung, L. Kovarik, Z. Wang, T. J. Roosendaal, Z. Zhu, D. J. Edwards, S. Y. Hu, C. H. Henager, Jr., R. J. Kurtz, and Y. Wang, J. Nucl. Mater. 458 (2015) 146.
[3] J. F. Ziegler, J. P. Biearsack, and U. Littmark, The stopping and Range of Ions in Solids (Pergamon Press, New York, 1985); available from: http://www.SRIM.org/.
[4] Y. Chen, P. H. Chou, E. A. Marquis, J. Nucl. Mater. 451 (2014) 130.
[5] Z. Jiao, G. S. Was, Acta. Mater. 59 (2011) 1220.
[6] M. K. Miller, R. G. Forbes, *Atom-Probe Tomography: The Local Electrode Atom Probe*, Springer, 2014.
[7] B. Gault, M. P. Moody, J. M. Cairney, S. P. Ringer, *Atom Probe Microscopy*, Springer, 2012.